

Evidences for Different Reaction Sites for Dehydrogenation and Dehydration of Ethanol over Vanadia Supported on Titania

Yu Kwon Kim[†] and Seol Ryu^{‡,*}

[†]Department of Chemistry and Department of Energy Systems Research, Ajou University, Suwon 16499, Republic of Korea

[‡]Department of Chemistry, Chosun University, Gwangju 61452, Republic of Korea.

*E-mail: sryu@chosun.ac.kr

Received February 26, 2019, Accepted March 11, 2019, Published online April 29, 2019

Vanadia supported on titania were prepared with increasing vanadia loadings up to 20 wt % to study the effect of the vanadia loading on catalytic reactivity. A competitive decomposition of ethanol into ethylene (dehydration) and acetaldehyde (dehydrogenation) over the catalyst occurs over the vanadia supported on TiO₂. Dehydrogenation is generally favored over dehydration over a wide range of the vanadia loadings up to 20 wt % due to a lower energy barrier for the dehydrogenation channel. Both dehydration and dehydrogenation rates are enhanced in proportion to the vanadia loadings up to about 2 wt %. At higher vanadia loadings (>2 wt %), however, the dehydration rate decreases while the dehydrogenation rate saturates. X-ray photoelectron spectroscopic analysis reveals that reduced V and Ti species are formed at the low vanadia contents and act as strong dissociative adsorption sites for H₂O, while extended VO_x clusters as well as three-dimensional V₂O₅ islands formed at high vanadia loadings prevent the formation of such sites. Thus, the observed difference between the two reaction channels can be explained from the structural transition of the vanadia overlayers from highly dispersed small VO_x clusters into larger polyvanadates or islands. At low vanadia loadings (<2 wt %), both the edge sites and the surface sites of the small VO_x clusters grow in proportion to the loadings as the number of the clusters increases. Thus, both reaction channels are enhanced as well. At higher vanadia loadings (>2 wt %), however, the transformation into larger islands reduces the edge sites or the boundaries between the clusters and TiO, not the surface area. This implies that the active sites for the dehydrogenation are on the surfaces of the vanadia overlayers, while those for the dehydration are on the boundaries between the VO_x and TiO₂. Our results provide an additional insight into the active sites for dehydration and dehydrogenation reactions over the titania-supported vanadia catalysts.

Keywords: Vanadia/TiO₂, Dehydrogenation, Dehydration, Ethanol

Introduction

Titania-supported vanadia (VO_x/TiO₂) catalysts are commercial materials that are used for the removal of NO_x by selective catalytic reduction with ammonia.^{1–5} Also, they are known to be active for various reactions including oxidative dehydrogenation (ODH) of alkane^{6–10} and alcohols such as methanol^{11,12} and ethanol.^{13–16} Especially, increasing interests on the use of ethanol as a fuel or a feedstock to produce hydrogen have triggered many studies on the use of various vanadia-based catalysts for the conversion of ethanol into acetaldehyde or ethylene, with modified supports such as TiO₂-SiO₂,^{17,18} ZrO₂-SiO₂,¹⁹ Al₂O₃,¹³ and with promoters such as alkali metals.^{16,20}

One of the key factors determining the catalytic activity is the structure of vanadium oxides in the supported vanadia catalysts, which would vary with the vanadia loading and the type of interaction with the supporting oxide. Vanadium oxides can exist as isolated vanadium oxide

species,^{21–23} a polymeric vanadium oxide species,^{23,24} and crystalline vanadium oxide species.^{25,26} Studies of Kilos *et al.*, indicate that VO_x species from monovanadate to polyvanadate structures are formed with increasing vanadia loadings, which would grow into crystalline V₂O₅ domains at higher vanadia loadings.¹³ Here, the interaction with the support determines not only the types of vanadium oxide species^{21,23,27} but also the catalytic activity, which can vary by orders of magnitude.^{28,29} Highly selective (~80%) ODH of ethanol to acetaldehyde is suggested to occur on supported vanadia catalysts with a polyvanadate monolayer.^{13,30} Such diverse structures of supported vanadia catalysts also act a central role in tuning the surface acidity,^{1,31,32} such as Brønsted³² and Lewis acid,³³ which are also closely correlated with the nature of active sites in connection with surface V=O bonds³⁴ and specific influences of oxide supports.³⁵

In this study, we investigate into how selectivity and reactivity of ethanol toward dehydrogenation and

dehydration change for vanadia supported on TiO₂ (p-25) with increasing vanadia loadings up to 20 wt %. We find an enhancement of dehydration as well as dehydrogenation at low vanadia contents (0.3–2 wt %), which we attribute to an increased concentration of charged defects at/near the surface. Reactivity toward dehydrogenation is greatly enhanced with increasing vanadia loadings up to 2 wt % and saturates at higher vanadia loadings. We explain the observed variations in reactivity and selectivity from the changes in the density and distribution of the charged defects with increasing VO_x densities on TiO₂.

Experimental

Preparation of VO_x/TiO₂. Preparation of VO_x/TiO₂ catalysts (VO_x-p25) was performed by impregnation of the commercial TiO₂ (Degussa p-25, 47 m²/g) powders (1 g) with a concentrated nitric acid (14 M) solution containing 0–0.322 g of NH₄VO₃ (Sigma Aldrich, 99.0%) for the vanadia loadings of 0–20 wt %. The resulting solution was heated at 80 °C with a constant stirring for several hours, washed and dried at 100 °C for 10 h. After a final calcination under an O₂ flow at 500 °C, the resulting powders showed colors ranging from yellow to orange depending on the vanadia loading.

Characterization of VO_x/TiO₂. Characterization of VO_x/TiO₂ was performed by X-ray fluorescence (XRF), X-ray diffraction (XRD), UV–Vis diffuse reflectance spectroscopy (DRS) and X-ray photoelectron spectroscopy (XPS). The vanadia loading (wt %) used in the present study was determined from XRF analysis (Rigaku, TX, USA, ZSX Primus). The surface vanadium atomic density (~1.4 V atoms/nm²) of our VO_x-p25 for the vanadia loading of 1 wt % was also determined using the measured surface area of Degussa p-25 (47 m²/g, our measurement). XRD patterns of the VO_x-p25 were obtained using an X-ray diffractometer (Rigaku, TX, USA, Ultima III) with Cu-Kα (λ = 0.15406 nm, 40 kV, 30 mA) irradiation by scanning 2θ from 10° to 70° at a scanning speed of 2°/min to determine the appearance of any bulk vanadia phase as well as the crystallinity of our catalysts. UV–Vis DRS of the VO_x-p25 catalysts was obtained on a double-beam UV spectrophotometer (Scinco, Seoul, Korea, Neosys-2000) equipped with a BaSO₄-coated integrating sphere. The absorbance in the photon energies of 200–800 nm was measured for the determination of the band-gap (E_g) of our powder samples by applying the Kubelka-Munk model (that is, a plot of (F(R)hν)^{1/2} vs. hν). XPS measurements were performed in a XPS system (PHI, MN, USA, 5000 VersaProbe II) with Mg Kα (1253.6 eV) and a charge neutralization system. The binding energies are referenced to the C 1 s peak at 284.4 eV of the surface adventitious carbon.

Thermal Reactivity Measurements. Thermal reactivity measurements of ethanol over the VO_x-p25 catalysts were evaluated by gas chromatography (GC) (Younglin, Anyang-si, Korea Acme 6000MC) equipped with a column

(Porapak Q, Agilent, CA, USA, 6 ft) and a thermal conductivity detector detector, operating at a He flow of 20 sccm. Thermally vaporized ethanol in a bottle placed in a water bath maintained at 10 °C, was carried out in a He flow (40 sccm, net ethanol flux = 55 μmol/min) with O₂ (2 sccm, 82 μmol/min). The catalyst powder (0.1 g) was placed in a Pyrex tube reactor (Kwangjin Glass, Korea) and the temperature of the reactor was controlled from room temperature up to 400 °C by a ceramic heating jacket. The reactant gas passed through the tube reactor and the composition of the gas mixture after the reaction was analyzed by GC. A typical GC spectrum (Figure 1) indicates well-resolved signals for O₂, ethylene, H₂O, acetaldehyde, and ethanol. All the GC signals for the reactant and products were found to increase proportional to the reactant gas flux under our experimental condition, indicating that the reactions are not limited by the mass transfer limit. The absolute fluxes (μmol/min) of reaction products (ethylene and acetaldehyde) were determined by referencing the integrated GC peak area of a known flux of each gas. The integrated area of the GC peak was proportional to the concentration of each component in the gas flow.

Results and Discussion

Figure 2 shows XRD spectra for VO_x-p25 with selected vanadia loadings of 0, 2, 5, and 20 wt %. We find that the XRD peaks assigned to p-25 (associated with anatase and rutile TiO₂ phases) have no change in the peak position as well as in the intensity ratio with increasing vanadia loadings except a gradual decrease of the overall peak intensity due to the decrease in the mole ratio of p-25 in the composition of our catalysts. At the same time, new set of XRD peaks are observed from 5 wt %, which are assigned to orthorhombic crystalline V₂O₅ phase. Below 5 wt %, we find no distinct vanadia-related XRD feature within our detection limit; this implies that well-dispersed small VO_x clusters are uniformly dispersed over the TiO₂ support.

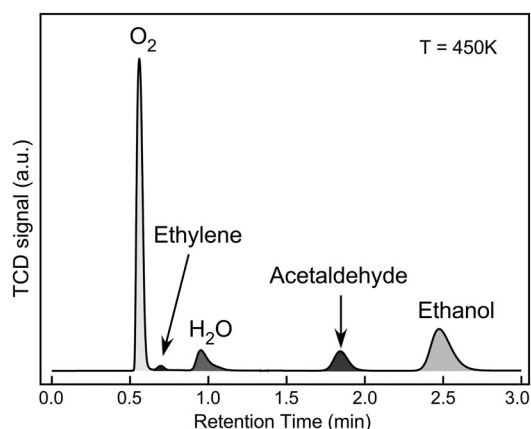


Figure 1. A typical GC spectrum showing all chemical species identified from our reactant gas (ethanol + O₂ in he flow) passed through VO_x-p25 catalysts at 450 K.

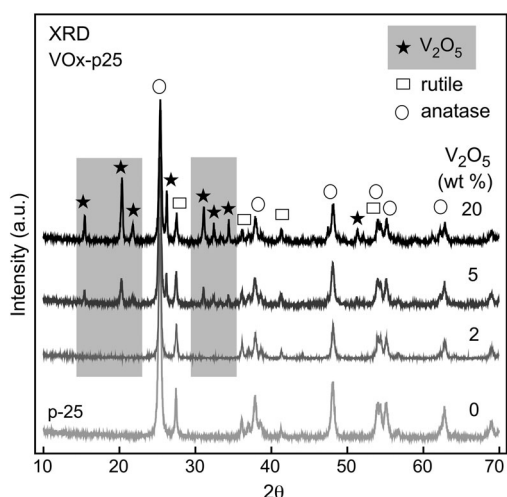


Figure 2. XRD patterns of VO_x-p25 prepared with the vanadia loadings of 0, 2, 5, and 20 wt %. XRD peaks for bulk crystalline V₂O₅ phase are noted for V-loading of 5 and 20 wt %.

Figure 3 shows the band gap of our VO_x-p25 catalysts determined from the UV-vis DRS measurements. We find that the band gap of p-25 (~3.0 eV) decreases in proportion to the vanadia loading from the very early stage and slowly approaches to about 1.7 eV above the vanadia loading of about 10 wt %. A gradual increase in the domain size of surface vanadia overlayers in a form of polyvanadate would induce a gradual shift in the absorption edge in the UV-vis spectra.³⁶ Compared with the band gap of bulk crystalline V₂O₅ (2.2 eV), the band gap goes below 2.0 eV at above 5 wt % of vanadium. This indicates the formation of disordered structure of VO_x clusters on TiO₂ with possible V incorporation into TiO₂ in addition to large crystalline bulk V₂O₅ islands (which is confirmed from XRD in Figure 2).

During the cycles of reactions up to 570 K, the colors of our catalysts remain unchanged as determined by naked eyes and the reactivity is maintained to be constant over cycles, suggesting that our reaction condition does not change the surface or bulk structure of our catalysts. In addition, we find H₂O desorption as a dominant byproduct;

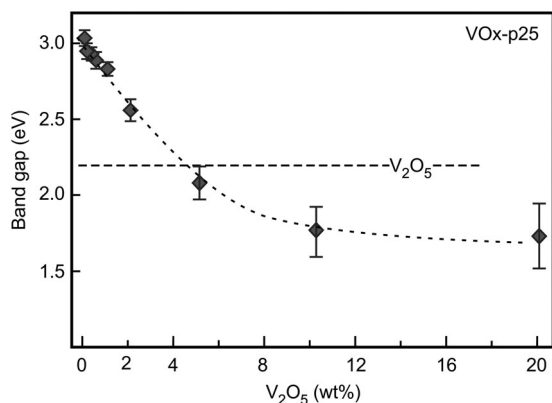


Figure 3. The band gap of VO_x-p25 plotted against the vanadia loading (wt %). Dotted line is to guide the eyes.

no H₂ desorption is detected up to 570 K. Thus, the following stoichiometric reactions of dehydrogenation and dehydration are suggested as described below;

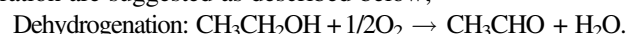


Figure 4 shows the areal rates of dehydrogenation (top) and dehydration (bottom) with increasing vanadia loadings at selected temperatures between 380 and 460 K. Both reactions are greatly enhanced with increasing temperatures. In addition, the enhancement is in proportion to the vanadium loading from the very initial content. A difference between the two channels is also found; the dehydrogenation rate saturates at the vanadia loadings of 2 wt % and above, while the dehydration rate, shows a maximum at 2 wt %, then decreases at higher vanadia loadings. The ratio between the two channels (dehydrogenation/dehydration) is higher than 50 at the very low vanadia loading (~0.1 wt %), indicating the selectivity is in favor of dehydrogenation. But it gradually decreases to about 20 as the vanadia loading approaches to 2 wt %, then increases again to about 50 at 20 wt %.

The fact that the enhancement starts from the very initial vanadia loading up to 2 wt % indicate that the initial vanadia overlayers provide the active sites for both reactions. These coverages (0–2 wt %) corresponds to those without distinct vanadia phase in XRD (Figure 2).

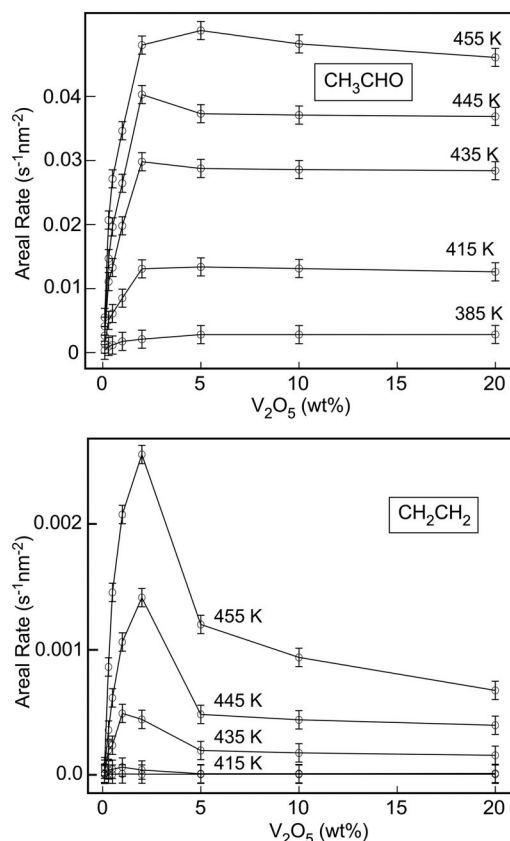


Figure 4. Areal rates (per s/nm²) of dehydrogenation and dehydration are plotted vs. the vanadia loading (wt %) at different temperatures.

Thus, highly dispersed VO_x clusters that can be formed in the low coverage ranges provide active sites for both reactions.

The difference in the behavior of the reaction rate enhancement between the two reaction channels at around 2 wt % suggests different active sites for both channels. It may be that *the active sites for dehydrogenation are on the surface layers of the vanadia islands, and those for dehydration are at the boundary sites of the islands*. Small vanadia islands are formed in the beginning and will grow in size at higher loadings. The surface area of the vanadia islands can be expected to grow and saturate at higher loadings even though the size of the islands grows later. The boundary sites (between TiO_2 and vanadia) will also increase in the beginning when small islands are formed at low vanadia loadings. However, they will begin to decrease

as the size of the islands grow at higher vanadia loadings (>2 wt %).

The measured reaction rates (in a unit of $\mu\text{mol}/\text{min}$) of acetaldehyde and ethylene, corresponding to dehydrogenation and dehydration, respectively, are plotted in the Arrhenius form of $\ln(R)$ vs. $1/T$, in Figure 5. The maximum conversion of ethanol into acetaldehyde (ethylene) measured in the present experiment is in the range of 0–10% (0–1%) for acetaldehyde (ethylene). A quite linear relation between $\ln(R)$ and $1/T$ is obtained for the reaction condition studied, suggesting that the reaction rates is not limited by the reactant.

The enhanced reaction rates or turnover frequencies with increasing vanadia loadings are reflected as a shift of the linear relation in the Arrhenius plot (Figure 5) toward lower temperatures. For dehydrogenation, the low-temperature shift saturates above 2 wt %, while it shifts back to higher temperatures by about 20 K above 2 wt % for dehydration. This is consistent with the reduced reaction rates for dehydration at higher vanadia loadings as indicated in Figure 4.

We can also determine the apparent energy barrier (ΔE_{app}) from the slopes in the Arrhenius plot, as shown in Figure 6. For the dehydrogenation channel, they are measured to be $\sim 70 \pm 10$ kJ/mol at all vanadia loadings up to 20 wt %. This value is quite close to the experimentally determined energy barrier of methanol dehydrogenation over vanadia supported on TiO_2 .³⁷ For dehydration, however, they are measured to vary depending on the vanadia loading. The lowest value of ~ 140 kJ/mol is obtained at 0.1–0.3 wt %. ΔE_{app} , however, increases again with increasing vanadia loadings and saturates at 160–170 kJ/mol above 2 wt %. This value is somewhat close to 175 kJ/mol for ethanol dehydration over rutile $\text{TiO}_2(110)$ surface,³⁸ at which the oxygen vacancies with excess charges act as reaction sites for ethanol dehydration.³⁹ The higher ΔE_{app} for p-25 (~ 200 kJ/mol) may be due to the fact that oxygen vacancies need to be created on fully oxidized p-25 for ethanol dehydration.

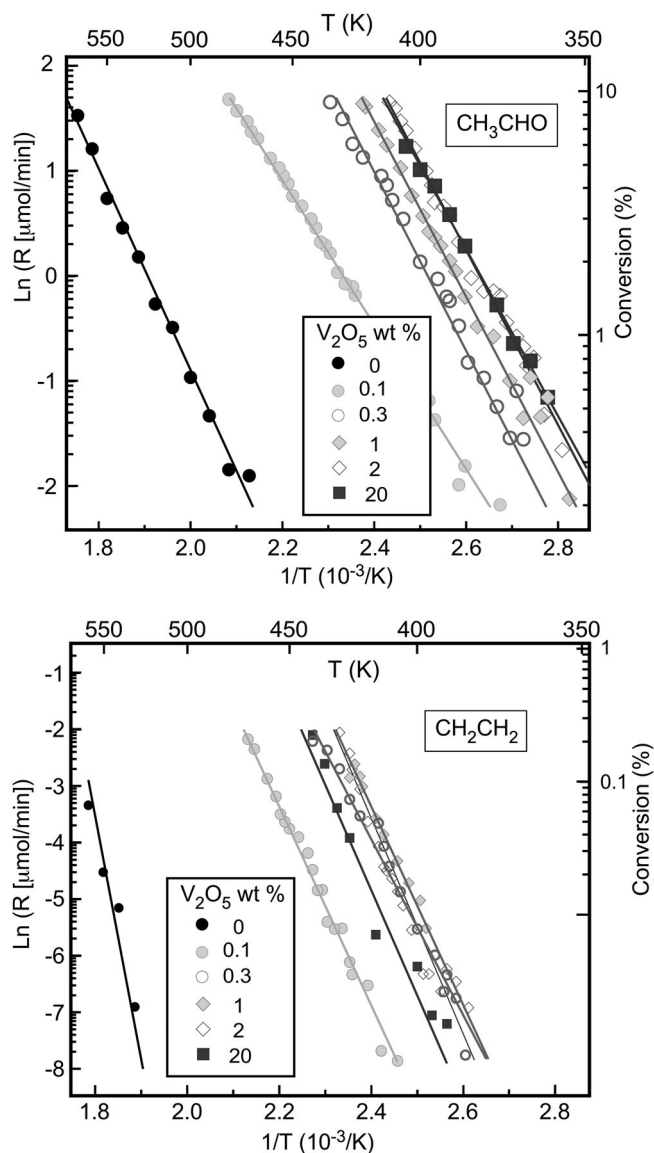


Figure 5. Arrhenius plot for dehydrogenation (top) and dehydration (bottom) of ethanol over $\text{VO}_x\text{-p25}$ with the vanadia loadings of 0–20 wt %.

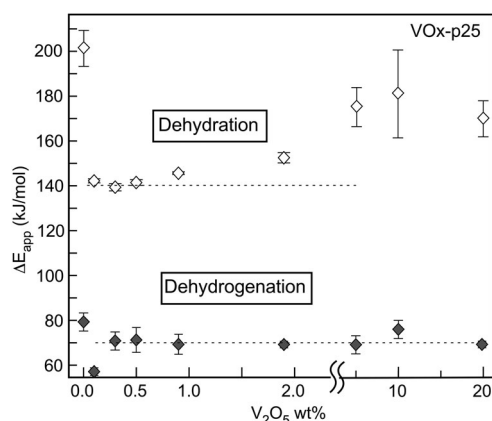


Figure 6. Apparent activation energy barriers for dehydration and dehydrogenation of ethanol over $\text{VO}_x\text{-p25}$.

Considering that the catalytic reactivity is not limited by the gas flow, the change in the measured ΔE_{app} is a direct measure of the energy barrier of a rate-limiting step. This leads to the conclusion that *the rate-limiting step for dehydrogenation is insensitive to the coverage of vanadia or the size of VO_x-p25, while that for dehydration is more structure-sensitive.* This result is consistent with our speculation that the active sites for dehydrogenation are on the surface of 2D vanadia islands while those for dehydration are on the boundaries of the islands. It is likely that the boundary sites are more sensitive to the size of the islands. Enhanced dehydrogenation over polyvanadates has been suggested in a recent study of others,¹³ suggesting that the active sites for dehydrogenation are on the surface of extended vanadia overlayers.

Chemical bonding states of our VO_x-p25 catalysts are further investigated from XPS analysis as shown in Figure 7. Here, Ti 2p, V 2p, and O 1s core level spectra are shown with increasing vanadia loadings. Ti 2p_{3/2} at 458.5 eV is from Ti⁴⁺ species in the bulk TiO₂.^{40–42} In addition to the major Ti⁴⁺ species, a shoulder feature appears toward lower binding energy at the vanadia loadings of 0.3–0.5 wt % (indicated by arrows), which can be assigned to a reduced Ti species such as Ti³⁺ as in Ti interstitials⁴² or Ti₂O₃.^{43,44} At higher vanadia loadings (5–20 wt %), the main Ti 2p_{3/2} peak decreases in intensity due to the formation of three-dimensional crystalline V₂O₅ islands.

V 2p_{3/2} features starts to appear at 515–516 eV from 0.3 vanadia wt %, which shifts to 517 eV as the vanadia loading increases above 2 wt %. The main V 2p_{3/2} peak at 517 eV is assigned to V⁵⁺ species from the bulk V₂O₅ phase^{40,45} in V₂O₅/TiO₂.^{46,47} The V 2p_{3/2} features at lower binding energies (516–515 eV) at the very low vanadia loadings are due to reduced V species such as V⁴⁺,^{40,48,49} and V³⁺.^{40,50} The reduced V species can originate from highly dispersed VO_x clusters or V species incorporated into the TiO₂ lattice (substituted for Ti⁴⁺).⁵¹

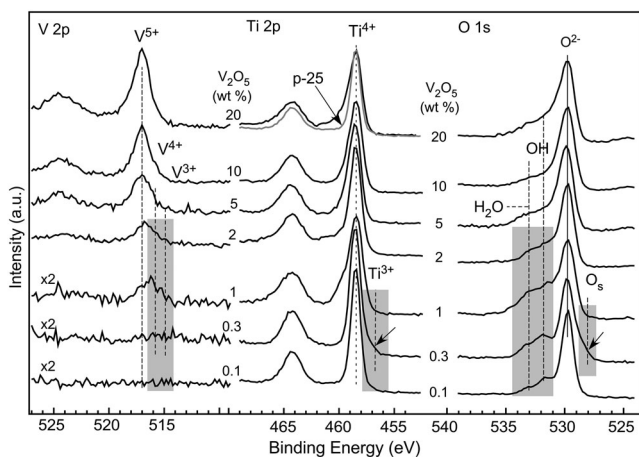


Figure 7. V 2p, Ti 2p, and O 1s core level spectra of VO_x-p25 catalysts with increasing vanadia loadings.

The main O 1s peak at 529.8 eV is due to the lattice oxygen species in TiO₂. The O 1s binding energy of bulk V₂O₅ also appears at a very similar position^{40,41} and little shift in O 1s peak position is observed with increasing vanadia loadings. The shoulder features toward higher binding energies (with distinct peaks at 532 and 533 eV, observed especially at 0.1–0.5 vanadia wt %) are assigned to surface-bound OH⁴³ and H₂O species, respectively, as has been reported on vanadia,⁵² TiO₂,^{53,54} and VO_x/TiO₂.⁴⁸ The shoulder feature (labeled as O_s, at 528.5 eV) toward lower binding energies of the main O 1s peak observed especially at 0.3–0.5 V₂O₅ wt % (indicated by arrows) may be due to surface O atoms bound to reduced Ti sites as has been reported on VO_x/TiO₂⁵⁰ as well as on reduced titania,^{43,55} in a form of O²⁻.⁵⁶

Figure 8 shows the XPS-determined surface atomic concentration ratio of Ti and V of our VO_x-p25 catalysts with increasing vanadia loadings. A linear increase (decrease) of V (Ti)-ratio up to 2 wt % indicates a growth of highly dispersed VO_x clusters on TiO₂. A deviation from the linearity occurs indicates a growth of three-dimensional large V₂O₅ islands on TiO₂.

Based on the above XPS analysis, it is clear that highly dispersed (and reduced) V species on TiO₂ surface are formed at 0–2 wt %. Strong interaction between vanadia and titania^{57,58} and the disordered structure of the surfaces of p-25 nanoparticles inhibit the transformation of isolated VO_x clusters into polyvanadates or even three-dimensional V₂O₅ islands up to the vanadia loading of 2 wt % (or 2.8 V/nm²). The reduced V species (V⁴⁺ and V³⁺) are suggested to be stabilized on the surface of titania.^{58,59} The reduced V species on titania-supported vanadia could exist in various forms such as a single or an extended VO_x clusters with terminal vanadyl group (V=O),^{12,35,60–62} VO₂,⁴⁹ V₂O₃,^{50,63,64} or V species incorporated into the TiO₂ lattice substituting lattice Ti⁴⁺ in a form of Ti-O-V.⁶⁵ Incorporation of such V species into the TiO₂ lattice can occur during calcination above 450 °C,⁶⁶ and would induce charged defects into the bulk.

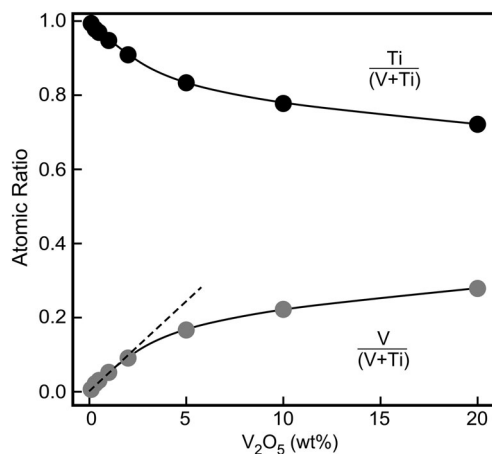


Figure 8. Surface atomic ratio of Ti and V determined from integrated areas of Ti 2p and V 2p core levels in Figure 7.

O 1 s spectra in Figure 7 also indicate that surface O, OH, and H₂O contents are higher at low vanadia loadings (0.1–2 wt %), suggesting that the highly dispersed V species formed on TiO₂ can act as stable binding sites for those oxygen species. The growth of polyvanadates as well as large crystalline V₂O₅ islands (XRD in Figure 2) at high vanadia loadings reduces the binding sites for surface OH and H₂O species. Thus, the binding sites for H₂O and OH are likely to be distributed to the boundaries between polyvanadates and TiO₂ as well as those of the isolated VO_x clusters. Such VO_x species are reported to be in a form of a vanadium atom with a vanadyl group (V=O) and oxygen atoms (in a distorted tetrahedral geometry) that bridge the vanadium atom to the Ti atoms in the TiO₂ support.^{67,68} Binding sites for H₂O can also act as the binding sites for alcohol (RO–H).

Ethanol may dissociate into ethoxy (CH₃CH₂O) and hydroxyl (OH) over terminal vanadyl group or over reduced Ti (or V) sites.^{13,69} Hydroxyls recombinatively desorb from the surface as H₂O^{13,70}; this process consumes lattice oxygen in the oxide catalyst and needs to be replenished from O₂ gas to keep the stoichiometric cycles of catalytic reaction. Ethoxy can be released from the surface by a rate-limiting decomposition into acetaldehyde (α -H elimination) or ethylene (β -H elimination).^{13,38}

Combining the results of XPS (Figure 7) and reactivity analysis (Figures 4 and 5), we conclude that the presence of reduced V (or Ti) species on/near the surface at the low vanadia loadings is the origin of the enhanced reactivity and selectivity, especially in favor of dehydration. The reduced V (or Ti) species provide excess charges to the surface in various forms of point defects such as interstitials and oxygen vacancies.⁶⁶ The role of such defects in catalyzing catalytic dehydrogenation and dehydration has been extensively studied over rutile TiO₂(110) surface^{71,72} as well as on a V-deposited TiO₂ surface.⁵⁸ The decrease in the apparent energy barrier of dehydration at low vanadia loadings also explains a direct influence of the defects in lowering the energy barrier for the rate-limiting step (β -H elimination) toward dehydration. No or negligible effect of the vanadia loading on the energy barrier of dehydrogenation suggests the insensitivity of the reaction pathway for dehydrogenation to the charged defects. Here, the role of the vanadyl group (V=O) in the surface VO_x clusters is regarded to be important.^{12,73–75}

As the TiO₂ is saturated with VO_x clusters with increasing surface VO_x density, dispersed (mono) VO_x clusters are connected by V–O–V linkages to form extended (poly) vanadates (or even three-dimensional V₂O₅ islands). Suppression of dehydration at the higher VO_x density is expected to be the result of decreased number of active sites associated with reduced V (or Ti) sites, which may be located on/near the edges of the isolated VO_x clusters as well as on bare TiO₂ surfaces. The formation of polyvanadate overlayers reduce the number of edge sites with charged point defects (e.g., oxygen vacancies and reduced V or Ti species) at the

interface between VO_x clusters and TiO₂ surface due to the reduced boundary sites of larger vanadia islands.

Conclusion

To summarize our results, ethanol dehydrogenation is found to be favored over dehydration on our titania-supported vanadia catalysts. At the very low vanadia loading, we find that the surface has a high density of reduced Ti (or V) species with highly dispersed small VO_x clusters. Such defective structures provide strong binding sites not only for H₂O dissociation into OH, but also for alcohols for heterolytic dissociation into alkoxy and OH for oxidative and reductive catalytic reactions into aldehyde and alkene, respectively. At higher vanadia loadings, the growth of extended VO_x structures such as polyvanadates and large V₂O₅ islands suppress the formation of such defective structures, which reduces the dehydration channel. The structure insensitivity of the dehydrogenation suggests the active sites are on the surface of vanadia. We find that the structural transition from small VO_x clusters into larger islands play a key role in controlling the reactivity and selectivity in catalytic reactions of ethanol.

Acknowledgments. This research was supported by Basic Science Research Program through the National Research Foundation of Korea (NRF) funded by the Ministry of Education, Science and Technology (NRF-2016R1D1A1B03931639) and the Human Resources Development of the Korea Institute of Energy Technology Evaluation and Planning (KETEP) grant funded by the Korea government Ministry of Trade, Industry & Energy (No. 20154010200820).

References

1. C.-H. Lin, H. Bai, *Appl. Catal. B Environ.* **2003**, *42*, 279.
2. I. Giakoumelou, C. Fountzoula, C. Kordulis, S. Boghosian, *J. Catal.* **2006**, *239*, 1.
3. F. Tang, B. Xu, H. Shi, J. Qiu, Y. Fan, *Appl. Catal. Environ.* **2010**, *94*, 71.
4. Q. Li, H. Yang, F. Qiu, X. Zhang, *J. Hazard. Mater.* **2011**, *192*, 915.
5. P. H. Mutin, A. F. Popa, A. Vioux, G. Delahay, B. Coq, *Appl. Catal. Environ.* **2006**, *69*, 49.
6. M. V. Martínez-Huerta, X. Gao, H. Tian, I. E. Wachs, J. L. G. Fierro, M. A. Banares, *Catal. Today* **2006**, *118*, 279.
7. A. A. Lemonidou, L. Nalbandian, I. A. Vasalos, *Catal. Today* **2000**, *61*, 333.
8. R. Grabowski, B. Grzybowska, A. Kozłowska, J. Słoczyński, K. Weislo, Y. Barbaux, *Top. Catal.* **1996**, *3*, 277.
9. A. Adamski, Z. Sojka, K. Dyrek, M. Che, G. Wendt, S. Albrecht, *Langmuir* **1999**, *15*, 5733.
10. M. D. Argyle, K. Chen, A. T. Bell, E. Iglesia, *J. Catal.* **2002**, *208*, 139.
11. P. Forzatti, E. Tronconi, A. S. Elmi, G. Busca, *Appl. Catal. Gen.* **1997**, *157*, 387.

12. H. Y. Kim, H. M. Lee, R. G. S. Pala, H. Metiu, *J. Phys. Chem. C* **2009**, *113*, 16083.
13. B. Kilos, A. T. Bell, E. Iglesia, *J. Phys. Chem. C* **2009**, *113*, 2830.
14. R. Tesser, V. Maradei, M. Di Serio, E. Santacesaria, *Ind. Eng. Chem. Res.* **2004**, *43*, 1623.
15. J. H. Kwak, J. E. Herrera, J. Z. Hu, Y. Wang, C. H. F. Peden, *Appl. Catal. Gen.* **2006**, *300*, 109.
16. R. J. Chimentão, J. E. Herrera, J. H. Kwak, F. Medina, Y. Wang, C. H. F. Peden, *Appl. Catal. Gen.* **2007**, *332*, 263.
17. E. Santacesaria, A. Sorrentino, R. Tesser, M. Di Serio, A. Ruggiero, *J. Mol. Catal. A Chem.* **2003**, *204*, 617.
18. N. E. Quaranta, J. Soria, V. C. Corberán, J. L. G. Fierro, *J. Catal.* **1997**, *171*, 1.
19. Y.-C. Lin, C.-H. Chang, C.-C. Chen, J.-M. Jehng, S.-G. Shyu, *Cat. Com.* **2008**, *9*, 675.
20. M. Calatayud, C. Minot, *J. Phys. Chem. C* **2007**, *111*, 6411.
21. T. Tanaka, H. Yamashita, R. Tsuchitani, T. Funabiki, S. Yoshida, *J. Chem. Soc. Faraday Trans. 1* **1988**, *84*, 2987.
22. H. Eckert, I. E. Wachs, *J. Phys. Chem.* **1989**, *93*, 6796.
23. Z. Luan, P. A. Meloni, R. S. Czernuszewicz, L. Kevan, *J. Phys. Chem. B.* **1997**, *101*, 9046.
24. G. G. Cortez, M. A. Bañares, *J. Catal.* **2002**, *209*, 197.
25. J. P. Balikdjian, A. Davidson, S. Launay, H. Eckert, M. Che, *J. Phys. Chem. B.* **2000**, *104*, 8931.
26. J. Spengler, F. Anderle, E. Bosch, R. K. Grasselli, B. Pillep, P. Behrens, O. B. Lapina, A. A. Shubin, H. J. Eberle, H. Knözinger, *J. Phys. Chem. B.* **2001**, *105*, 10772.
27. V. Brázdová, M. V. n. Ganduglia-Pirovano, J. Sauer, *J. Phys. Chem. C* **2010**, *114*, 4983.
28. I. E. Wachs, *Catal. Today* **2005**, *100*, 79.
29. G. T. Went, L.-J. Leu, R. R. Rosin, A. T. Bell, *J. Catal.* **1992**, *134*, 492.
30. G. C. Bond, S. F. Tahir, *Appl. Catal.* **1991**, *71*, 1.
31. H. Schneider, S. Tschudin, M. Schneider, A. Wokaun, A. Baiker, *J. Catal.* **1994**, *147*, 5.
32. N. Y. Topsoe, J. A. Dumesic, H. Topsoe, *J. Catal.* **1995**, *151*, 241.
33. L. Lietti, J. L. Alemany, P. Forzatti, G. Busca, G. Ramis, E. Giamello, F. Bregani, *Catal. Today* **1996**, *29*, 143.
34. I. E. Wachs, *Catal. Today* **1996**, *27*, 437.
35. B. Olthof, A. Khodakov, A. T. Bell, E. Iglesia, *J. Phys. Chem. B.* **2000**, *104*, 1516.
36. A. Khodakov, B. Olthof, A. T. Bell, E. Iglesia, *J. Catal.* **1999**, *181*, 205.
37. J. L. Bronkema, D. C. Leo, A. T. Bell, *J. Phys. Chem. C* **2007**, *111*, 14530.
38. Y. Kim, B. Kay, J. M. White, Z. Dohnálek, *Catal. Lett.* **2007**, *119*, 1.
39. Y. K. Kim, B. D. Kay, J. M. White, Z. Dohnalek, *Surf. Sci.* **2008**, *602*, 511.
40. Q. Wang, R. J. Madix, *Surf. Sci.* **2001**, *474*, L213.
41. J. Pouilleau, D. Devilliers, H. Groult, P. Marcus, *J. Mater. Sci.* **1997**, *32*, 5645.
42. Y. K. Kim, S. Park, K.-J. Kim, B. Kim, *J. Phys. Chem. C* **2011**, *115*, 18618.
43. P. M. Kumar, S. Badrinarayanan, M. Sastry, *Thin Solid Films* **2000**, *358*, 122.
44. A. F. Carley, P. R. Chalker, J. C. Riviere, M. W. Roberts, *J. Chem. Soc. Faraday Trans. 1* **1987**, *83*, 351.
45. G. Silversmit, D. Depla, H. Poelman, G. B. Marin, R. De Gryse, *J. Electron Spectros. Relat. Phenomena* **2004**, *135*, 167.
46. M. Kobayashi, R. Kuma, S. Masaki, N. Sugishima, *Appl. Catal. Environ.* **2005**, *60*, 173.
47. J. P. Nogier, M. Delamar, *Catal. Today* **1994**, *20*, 109.
48. G. Silversmit, H. Poelman, D. Depla, N. Barrett, G. B. Marin, R. De Gryse, *Surf. Interface Anal.* **2006**, *38*, 1257.
49. M. Sambì, G. Sangiovanni, G. Granozzi, F. Parmigiani, *Phys. Rev. B* **1997**, *55*, 7850.
50. Q. Guo, S. Lee, D. W. Goodman, *Surf. Sci.* **1999**, *437*, 38.
51. X. Yang, C. Cao, K. Hohn, L. Erickson, R. Maghirang, D. Hamal, K. Klabunde, *J. Catal.* **2007**, *252*, 296.
52. V. Bondarenka, S. Grebinkij, S. Kaciulis, G. Mattogno, S. Mickevicius, H. Tvardauskas, V. Volkov, G. Zakharova, *J. Electron Spectros. Relat. Phenomena* **2001**, *120*, 131.
53. G. Philippin, J. Delhalle, Z. Mekhalif, *Appl. Surf. Sci.* **2003**, *212–213*, 530.
54. S. Kaciulis, G. Mattogno, A. Napoli, E. Bemporad, F. Ferrari, A. Montenero, G. Gnappi, *J. Electron Spectros. Relat. Phenomena* **1998**, *95*, 61.
55. C.-N. Huang, J.-S. Bow, Y. Zheng, S.-Y. Chen, N. Ho, P. Shen, *Nanoscale Res. Lett.* **2010**, *5*, 972.
56. J.-C. Dupin, D. Gonbeau, P. Vinatier, A. Levasseur, *Phys. Chem. Chem. Phys.* **2000**, *2*, 1319.
57. I. E. Wachs, B. M. Weckhuysen, *Appl. Catal. Gen.* **1997**, *157*, 67.
58. S. Lee, G. W. Zajac, D. W. Goodman, *Top Catal* **2006**, *38*, 127.
59. M. A. Bañares, L. J. Alemany, M. C. Jiménez, M. A. Larrubia, F. Delgado, M. L. Granados, A. Martínez-Arias, J. M. Blasco, J. L. G. Fierro, *J. Solid State Chem.* **1996**, *124*, 69.
60. B. M. Weckhuysen, D. E. Keller, *Catal. Today* **2003**, *78*, 25.
61. G. Centi, *Appl. Catal. Gen.* **1996**, *147*, 267.
62. V. Shapovalov, H. Metiu, *J. Phys. Chem. C* **2007**, *111*, 14179.
63. N. J. Price, J. B. Reitz, R. J. Madix, E. I. Solomon, *J. Electron Spectros. Relat. Phenomena* **1999**, *98–99*, 257.
64. E. A. Kröger, F. Allegretti, M. J. Knight, M. Polcik, D. I. Sayago, D. P. Woodruff, V. R. Dhanak, *Surf. Sci.* **2006**, *600*, 4813.
65. F. Trifirò, *Catal. Today* **1998**, *41*, 21.
66. J.-M. Herrmann, J. Disdier, G. Deo, I. E. Wachs, *J. Chem. Soc. Faraday Trans.* **1997**, *93*, 1655.
67. G. T. Went, L.-j. Leu, A. T. Bell, *J. Catal.* **1992**, *134*, 479.
68. X. Gao, I. E. Wachs, *J. Phys. Chem. B.* **2000**, *104*, 1261.
69. W.-C. Wu, C.-C. Chuang, J.-L. Lin, *J. Phys. Chem. B.* **2000**, *104*, 8719.
70. M. A. Henderson, *Langmuir* **1996**, *12*, 5093.
71. C. Lun Pang, R. Lindsay, G. Thornton, *Chem. Soc. Rev.* **2008**, *37*, 2328.
72. Z. Dohnálek, I. Lyubintsky, R. Rousseau, *Prog. Surf. Sci.* **2010**, *85*, 161.
73. R. Z. Khaliullin, A. T. Bell, *J. Phys. Chem. B.* **2002**, *106*, 7832.
74. H. Y. Kim, H. M. Lee, H. Metiu, *J. Phys. Chem. C* **2010**, *114*, 13736.
75. A. Goodrow, A. T. Bell, *J. Phys. Chem. C* **2008**, *112*, 13204.